Chemical Engineering Journal 380 (2020) 122524

Contents lists available at ScienceDirect

Chemical Engineering Journal

journal homepage: www.elsevier.com/locate/cej

Fabrication of meshes with inverse wettability based on the TiO_2 nanowires for continuous oil/water separation

Ziqiang Gong[1], Na Yang[1], Zhenxing Chen, Bin Jiang, Yongli Sun, Xiaodong Yang, Luhong Zhang*

School of Chemical Engineering and Technology, Tianjin University, Tianjin 300072, People's Republic of China

HIGHLIGHTS

- The construction of TiO_2 nanowires on stainless steel mesh has the advantage of low cost.
- A pair of meshes with inverse special wettability were fabricated via the successive steps.
- Various oil/water mixtures can be separated continuously with high efficiency and flux.
- The as-prepared mesh exhibited excellent stability in corrosive environments.

GRAPHICAL ABSTRACT

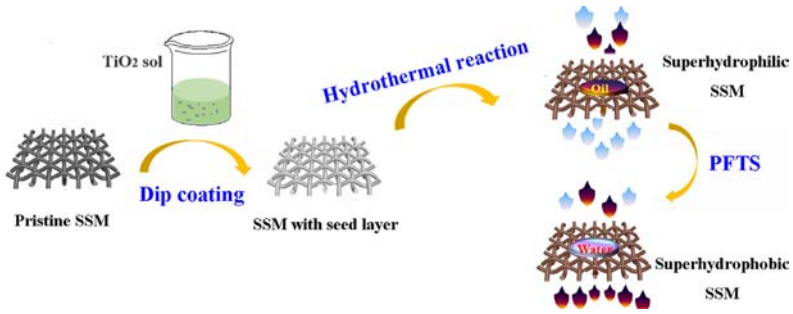

ARTICLE INFO

Keywords:
TiO_2 nanowires
Superhydrophilic
Superhydrophobic
Hydrothermal method
Oil/water separation

ABSTRACT

With the purpose of avoiding the limitation of oil/water density relationship, as well as achieving the continuous separation, two types of filtering materials with inverse wettability have attracted extensive attention. In our work, a superhydrophilic mesh was fabricated via a series of procedures, including the deposition of TiO_2 seed layer on the surface, the growth of TiO_2 nanowires by a hydrothermal method and calcination process. As expected, the as-prepared superhydrophilic mesh turned to be superhydrophobic after the decoration by low surface energy reagent. The formation mechanism of grass-like TiO_2 nanowires was proposed and surface morphological optimization conditions were studied. As for the oil/water application, the T-shaped bidirectional device combining the meshes with inverse wettability was adopted for achieving continuous oil/water separation. Meanwhile, the separation test showed that the separation efficiency of greater than 99% and high flux were obtained for various oil/water mixtures. Furthermore, according to the results simulating the realistic industrial application, the as-prepared meshes exhibited excellent reuse durability and stability in corrosive environment. The extension of TiO_2 nanowires on mesh, cooperating the multiple wettability behaviors could be regarded as a prospective candidate for large-scale oil/water separation.

1. Introduction

The oil/water mixture deriving from offshore crude oil leakage and oily wastewater discharge of industrial manufacture is partially in the form of immiscible type, which brings enormous challenge to the initial treatment, oil recovery and environmental protection [1–3]. Universally, owing to the maximum intrusion pressure accumulated by the intercepted phase and selectivity for relative density of oil and water, the material with single special wettability was employed to achieve separation process by the method of batch operation, which limits the

* Corresponding author.
E-mail address: zhanglvh@tju.edu.cn (L. Zhang).
[1] These authors contributed equally to this work.

https://doi.org/10.1016/j.cej.2019.122524
Received 14 May 2019; Received in revised form 14 July 2019; Accepted 15 August 2019
Available online 16 August 2019
1385-8947/

practical application. Therefore, it is significant to devise a novel material possessing the inverse special wettability to separate oil/water mixture. Generally, the special wettability is the essence of these materials due to the diverse interfacial effects towards water and oil [4,5].

In 2004, inspired by the marvelous feature of lotus leaf surface in nature, Feng et al. first proposed the utilization of superhydrophobic/superoleophilic ("oil-removing") metallic mesh for oil/water separation [6]. Thereafter, the superhydrophobic filtering membrane materials have attracted wide attention owing to their potential capacity for selective absorption of oils from water [7], self-cleaning [8], anti-icing coating [9] and corrosion resistance. So far, a large quantity of exploited functional materials with superhydrophobicity have been fabricated and applied into oil/water separation, such as Mg-Al LDHs in situ growth on textile [10], SiO_2/epoxy resin coated filter paper [11], 3D nickle foam [12–14], etc. Due to the intrinsic property of superoleophilicity, an accumulated oil layer formed on superhydrophobic surface could cause the blockage of porous channels, resulting in a decrease in permeation flux and separation efficiency.

To solve the aforementioned problems, the superhydrophilic materials enlightened by fish scale ("water removing") were put forward in recent years. Recently, the co-deposition of TA and APTES on commercial membrane [15], electrospinning cellulosic membrane [16], cellulose hydrogel-coated colander [17,18], and crosslinked poly vinyl alcohol (PVA) coating [19,20], as environmentally friendly and low cost approaches, are rapidly flourishing to become desired candidate for oil/water separation with high efficiency. Though the as-designed materials were capable to separate the majority of light oils, it is not suitable for the heavy oils with a density greater than water. Besides, the poor robustness and lack of reusability in long-term repeated use may have turned out to be the main barriers for practical applications. Therefore, a pair of filtering materials with inverse wettability based on the same coating are urgently required to be prepared and integrated into the separation device, which have the potential to achieve continuous separation of oil/water mixtures regardless of the density relationship.

With respect to constructing the superhydrophilic filtering materials from pioneering concept, the inorganic materials with high surface energy were advocated to achieve the property of underwater superoleophobicity and enhance the antifouling performance [21]. In addition, the theory of Young's equation shows that the hydrophilic surface in the air exhibits oleophobicity underwater, and the introduction of hierarchical rough structure for hydrophilic amplification can achieve the underwater superoleophobicity [22]. Many versatile materials with hierarchical structure, including $Cu(OH)_2$ nanowires [23], ZnO nanoparticles [24,25], and flower-like WO_3 [26], were used to endow the substrate with desirable wettability of superhydrophilicity. Although these metal oxides coated filtering materials demonstrated a high separation efficiency for oil/water separation, challenges still exist. For instance, some simple metal oxide coatings have a weak adhesion to substrate and are not stable enough in corrosive environments. To date, TiO_2 [27] is expected to be applicable for multifunctional materials owing to its favorable physicochemical properties, UV-induced hydrophilicity, nontoxicity and excellent stability [28]. The approaches on UV-induced superhydrophilic TiO_2 have been reported for self-cleaning, anti-fog and other applications [29,30]. Moreover, constructing the TiO_2 nanostructure on Ti foam was also developed for oil/water emulsion separation [31]. However, the dark condition could result in the loss of surface superhydrophilicity and the titanium substrates used in study are usually expensive, which limit their practical application.

In our work, the TiO_2 nanowires coated superhydrophilic mesh was synthesized by the pre-deposition of TiO_2 seed layer [32], growth of TiO_2 nanowires [33] and heat treatment. According to the research, when calcination temperature reaches to 450 °C, TiO_2 crystal structure changes from amorphous state to anatase and maintains long-term superhydrophilic stability without the UV light [34]. Thus, the as-prepared mesh exhibited unexceptionable affinity to water and low adhesion toward various oil underwater, which is crucial to achieve the oil/water separation with high permeation flux and efficiency. Further, the superb nanowires arrangement could be stacked into a papillary structure via capillary interaction, which paves a way for the modification of low surface energy agent to realize superhydrophobicity [35]. Herein, 1H, 1H, 2H, 2H-perfluorodecyltriethoxysilane was crosslinked to the surface of TiO_2 nanowires via the covalent bond and wettability changed from superhydrophilic to superhydrophobic. By using the designed T-shaped device that integrated two meshes with inverse wettability, oil/water mixture could be separated continuously regardless of the relative oil/water density. Moreover, constructing the TiO_2 nanowires on stainless steel mesh has a lower cost compared with other substrates, such as titanium mesh and titanium foam. The reusability and long-term stability are obtained by both meshes, which exhibit the great application prospect in industrial oil/water separation.

2. Experimental

2.1. Materials

The stainless steel mesh (mesh number of 300) was purchased from the Hebei Jiangcheng Co., Ltd. Tetrabutyl titanate (TBT, analytical grade) was supplied by Tianjin Damao Chemical Reagent Factory. Diethanolamine (DEA) and hexadecyl trimethyl ammonium bromide (CTAB) were obtained from Kaimat Chemical Technology Co., Ltd. Ethanol, hydrogen peroxide (H_2O_2, 30%) and nitric acid (HNO_3, analytical grade, 65%-68%) were purchased from Shanghai Aladdin Biochemical Technology Co., Ltd. Melamine (> 99.5%) and 1H, 1H, 2H, 2H-perfluorodecyltriethoxysilane (PFDS, 97%) were obtained from Shanghai Miner Chemical Technology Co., Ltd. The sponge titanium was provided by Beijing Xingrongyuan Technology Co., Ltd. All the reagents were used without any purification.

2.2. Fabrication of the TiO_2 sol

The TiO_2 sol was prepared as the following processes [36]. Briefly, 17.2 ml TBT, 4.8 ml DEA and 1 g CTAB were dissolved in 67.3 ml of absolute ethanol, then stirred vigorously at ambient temperature for 2 h to obtain homogeneous solution. During the magnetic stirring, a mixture of 0.9 ml of deionized water and 10 ml of ethanol was added dropwise. Finally, the above alkoxide solution was hydrolyzed at room temperature for 2 h to obtain the TiO_2 sol.

2.3. Preparation of superhydrophilic mesh

The stainless steel mesh (SSM) with size of $3 \times 3\ cm^2$ used as substrate was ultrasonically cleaned with ethanol, acetone and deionized water in turn to remove the surface impurity and dried for further use. To obtain the mesh deposited with TiO_2 seed layer (SSM@SL), the cleaned meshes were dipped in the TiO_2 sol by employing a pulling impregnation machine, and the concrete operating parameters are shown in Table1. After TiO_2 sol layer was uniformly covered on the

Table 1
The operation parameters of the dip-coating process in TiO_2 sol.

Descending speed	Lifting speed	Lifting height	Immersion time	Residence time	Dipping number
1000 μm/s	600 μm/s	40 mm	120 s	80 s	1

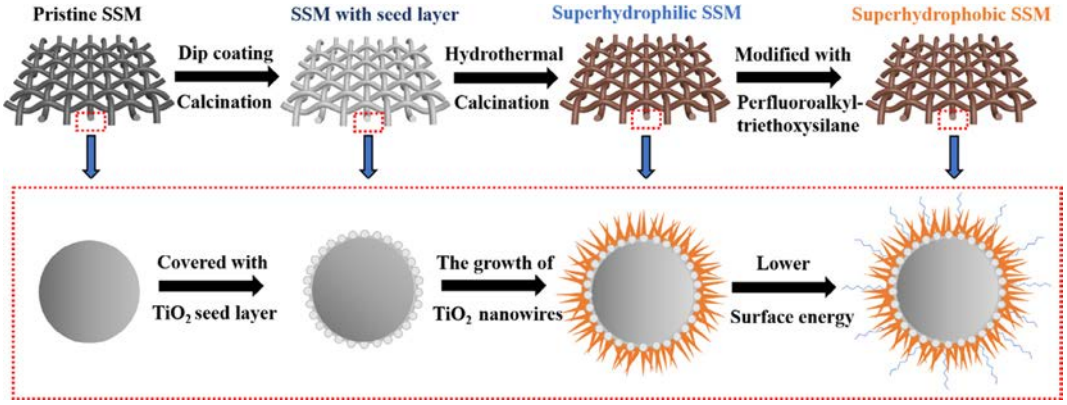

Scheme 1. Schematic illustration of formation process of superwetting mesh and cross section of the single wire.

mesh surface, it was incubated in muffle furnace at 450 °C for 1 h. Then, the obtained SSM@SL and sufficient titanium sponge were transferred into hydrothermal solution (containing 0.625 ml HNO_3, 0.0625 g melamine and 50 ml H_2O_2), in which TiO_2 nanowires were grown on the seed layer at 80 °C for 8 h [33,37]. After the hydrothermal reaction, the resulted meshes were washed with deionized water to remove the excessive deposits and further cured in muffle furnace at 450 °C for another 1 h. Finally, the superhydrophilic mesh (SSM@NWs) was obtained after cooling to room temperature.

2.4. Preparation of superhydrophobic mesh

The PFDS solution (1 wt%) was prepared by mixing a certain amount of PFDS in absolute ethanol, followed by adding 1 ml deionized water. Then the SSM@NWs was immersed in PFDS solution for 24 h to endow the surface with organic cross-linking layer, subsequently cured at 200 °C for 1 h. Finally, the superhydrophobic mesh (SSM@NWs-PFDS) was obtained via surface decoration process.

2.5. Oil/water separation

To efficiently separate kinds of oil/water mixtures, we integrated two types of superwetting meshes on both sides of T-shaped bidirectional device (Fig. 9). It is worth noting that the whole device was placed horizontally and the oil/water mixtures (1 L, 1:1, V/V) were pumped into upper tube via a peristaltic pump. The trace oil in the water phase was extracted by CCl_4 and then measured by the infrared oil detector. The Karl Fischer moisture meter was used to measure the trace oil content in the water phase. Moreover, the separation efficiency η was calculated by the formula:

$$\eta(\%) = \left(1 - \frac{C_1}{C_0} \times 100\%\right) \quad (1)$$

For the superhydrophobic side on the left, C_0 and C_1 represent the water content of original mixture and collected oil, respectively. As for the superhydrophilic side, the target concentration is the oil content.

The intrusion pressure P was defined as follows:

$$P = \rho g h_{max} \quad (2)$$

where ρ is the density of intercepted phase, g is the gravity and h_{max} represents the maximum height of intercepted phase. All the experimental data were determined as the average value of five measurements.

2.6. Characterization

The morphologies of SSM@NWs and SSM@NW-PFDS were observed by scanning electron microscopy (SEM, Nanosem430, USA). Raman information was obtained on DXR spectrometer (Thermo Fisher Scientific, USA) with the specific condition: the laser power of 5 mW, the excitation wavelength of 780 nm and integration time of 2 s. The sample data was captured in the range of 100–3300 cm^{-1}. The X-ray photoelectron spectroscopy (XPS, ULVACPHI, PHI 5000 VersaProbe) was performed to investigate the surface composition. All the binding energies were referenced to the standard value at 284.8 eV of C 1s peak. XRD (D8-Focus, AXS, Germany) spectra data was recorded at the 2θ of 5-60° with scanning rate of 8°/min using Cu Kα radiation (λ = 1.54056 Å). The contact angles of water or oil droplets on sample surface were acquired on an optical contact angle & interface tension meter (SL200KS, KINO, USA) with liquid volume of 5 μL. For contact angle measurement in air, the water or oil droplets were injected on flat surface of the as-prepared material. Then, the method of ellipse fitting was employed to calculate the contact angle values. The underwater wettability test was similar to the measurement in air.

3. Results and discussion

3.1. Materials and method

Scheme 1 demonstrates the continuous synthetic processes for SSM@NWs via a combined method of dip-coating and hydrothermal growth, constructing TiO_2 seed layer and nanowires on surface respectively. Ascribed to synergetic effect of nanowires roughness and abundant hydrophilic groups enhanced by the calcination treatment [34], the as-prepared SSM@NWs demonstrated unexceptionable characteristic of superhydrophilicity and underwater superoleophobicity. Moreover, the low surface energy is a critical factor for obtaining the superhydrophobicity, which could achieved by introducing the silane coupling agent or stearic acid [38]. The SSM@NWs reacted with PFTS to generate a dense organic layer of fluorinated alkyl chain crosslinked with covalent bond of Ti-O-Si, forming the superhydrophobic mesh. A comparative experiment was conducted to testify that the loss of crystal seed layer could be unfavorable to assembly of highly anisotropic nanowires structure (Fig. S1). Besides, the number of dipping coating has no particular impact on subsequent TiO_2 nanowires growth prior to seed layer deposition (Fig. S2), which illustrates that only one immersion treatment is sufficient to realize coverage of TiO_2 seed layer on surface thoroughly. Fig. S3 exhibits the conversion of surface morphology of the SSM@NWs prepared at 80 °C for different hydrothermal time: 4 h, 6 h, 8 h, and 10 h. When the reaction time was extended to 8 h, the deposited "TiO_2 transition layer" (hatching layer) reached a certain thickness and achieved a relatively uniform coverage, thus avoiding the phenomenon of cracking after calcination. Moreover, these two kinds of meshes reached the state of superhydrophobicity and underwater superoleophobicity, respectively. Considering the results based on the microscopic morphology (Fig. S3) and surface wettability, it is appropriate to determine the hydrothermal reaction time of 8 h as

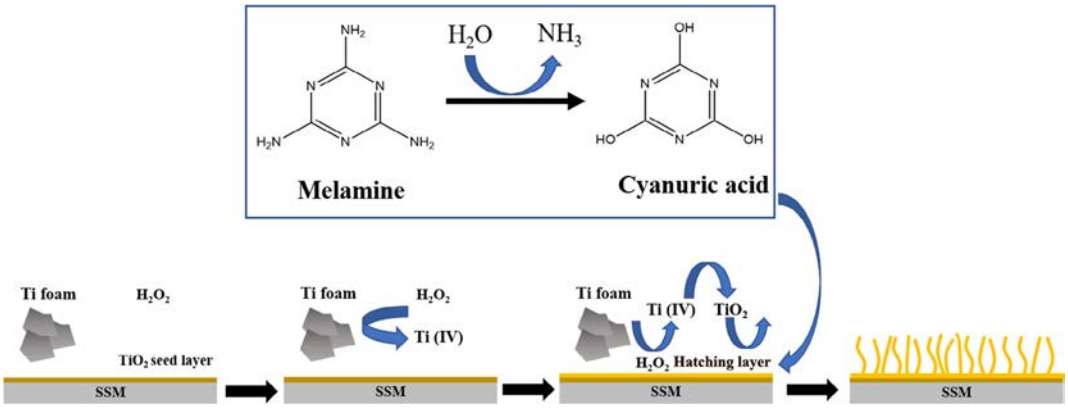

Scheme 2. Illustration for growth mechanism of the TiO_2 nanowires.

the optimal value. During the hydrothermal reaction, the formation mechanism of TiO_2 hierarchical micro/nano structure was shown in scheme 2. Firstly, titanium sponge was a titanium source in etching reaction, and interaction in Ti-H_2O_2 was actually a dissolution equilibrium process. Titanium sponge and hydrogen peroxide could react to form $Ti(OH)_4$, and the product is thermodynamically unstable and easily decomposes to form a TiO_2 sol, as shown in the following reaction [33].

$$Ti + H_2O_2 + 2H_2O = Ti(OH)_2O_2 + H_2 \quad (3)$$

$$Ti(OH)_2O_2 \rightarrow Ti(OH)O \rightarrow Ti(OH)_x \rightarrow TiO_2 \cdot nH_2O \quad (4)$$

Then, the Ti(IV) ions were released to solution through the dissolution of TiO_2 sol. Upon reaching to the critical concentration, the oversaturated Ti(IV) ions dispersed to SSM surface to form a TiO_2 thin layer, which act as an hatching layer. Notably, these hatching layer strengthened the adhesion between seed layer substrate and nanowires, so that nanowires could be anchored on the surface, which is beneficial to stability of separation application. Furthermore, the additive of HNO_3 could lower the pH of the system, stabilize the TiO_2 sol and reduce its nucleation in solution. Under such acidic condition, the hydrolysis of melamine was inferred to generate cyanuric acid and ammonia, further producing the NH_4^+ [33]. The "directed adsorption" of NH_4^+ on the crystal plane induced a ligand-directed assembly process as a consequence of highly heterogeneous nanowires structure.

To evaluate the applicability of the as-prepared meshes above, the intrusion pressure were calculated by the maximum height of water or oil that the as-prepared mesh can support. For SSM@NWs-PFDS, the results are shown in Fig. 1a, in which the water column dyed with methyl blue was intercepted by the porous superhydrophobic mesh, and maximum bearable height was measured to be 28.75 cm ± 0.45 cm corresponding to the intrusion pressure of 2.82 ± 0.04 kPa. Similarly, the intrusion pressure of oil for SSM@NWs was tested by employing the n-hexane (dyed with oil red) as sample oil (Fig. 1b). It can be seen that measured height was about 14.35 cm ± 0.25 cm and average intrusion pressure of oil was calculated to be 0.928 ± 0.02 kPa. It is worth noting that the as-prepared superhydrophilic mesh was supposed to be wetted by water in advance to guarantee the underwater superoleophobicity.

According to the results of the calculated maximum intrusion pressure, adopting the single mesh for oil/water separation could cause problems such as limited handing capacity and discontinuous operation. In our work, the detailed structure was designed as Fig. 2 and the superhydrophilic mesh should be wetted by water before separation. When the oil/water mixture flowed into the T-tube driven by peristaltic pump, the oil phase can only pass through the superhydrophobic side and the water phase can merely pass through the superhydrophilic side regardless of the oil/water density relationship. The specific oil/water wetting models and separation mechanism were discussed in Fig. S8. Consequently, the pure phase was found in the beakers without visible opposite phase, signifying the feasibility for practical oil/water separation.

3.2. Surface characterization

As shown in Fig. 3, the surface morphology variations of SSM before and after TiO_2 seed layer deposition were presented by SEM. The original mesh was intertwined by a large amount of metallic wires with average hole diameter of 50 μm (Fig. 3a), and surface is clean and smooth (Fig. 3c). After depositing the TiO_2 seed layer on the surface, it could be seen that hole channels of mesh were covered with TiO_2 film (Fig. 3b), because the excess sol in the immersion and pulling procedure formed a crystal layer between the voids and further undergone a calcination process. It is obvious that a relative roughness could be observed compared with original one (Fig. 3d). At high magnification, conglobate nanoparticles with size of 50–100 nm in diameter were coated on the surface (Fig. 3e–f), densely aligning to construct a seed layer on the mesh. During the subsequent growth process of nanowires on surface, the interfacial tension between the nucleation point and the solution ions depends on the matching degree between the nucleation point and the precipitation phase structure [39]. There is a similar structure between the precipitated phase and the deposited substrate after coating the SSM with seed layer, and the barrier among them is the lowest, which is beneficial to the growth of TiO_2 nanowires.

The surface morphologies at different magnifications as a result of hydrothermal reaction for 8 h were investigated by SEM imaging. After the hydrothermal reaction, partial cracks were observed in the gaps of the mesh (Fig. 4a), proving that the TiO_2 had been initially coated on the mesh. By magnifying, the cross-sectional view exhibited that the surface was uniformly wrapped by deposited TiO_2 (Fig. 4b). A mass of spherical papillaes (Fig. 4c) observed on the surface could be explained as crystal re-precipitation and secondary growth process in solid-liquid interface, which acts the preliminary micron-sized roughness. Further magnification reveals that the nanowire-like microstructure perpendicular to the surface is evenly distributed over the surface, as shown in Fig. 4d. Moreover, there is a hatching layer between the nanowires and seed layer, and thickness is about 0.5 μm (Fig. 4e), indicating an intensive combination among the multilayers. The interlaced nanowires were in grass-like shape with an average length of 1 μm (Fig. 4f). Theoretically, the rough surface with the nanowire structure could storage a large amount of air or water among the nanowires to form an air layer or a water layer, providing the necessary microstructure for the construction of the special wettability surface.

As shown in Fig. 5a, the apparent surface of the as-prepared mesh is brown. The XRD patterns were recorded to analysis the crystal configuration of the deposited TiO_2. The two characteristic peaks of the red line located at 43.7° and 50.9° are the diffraction peaks of the (1 1 1)

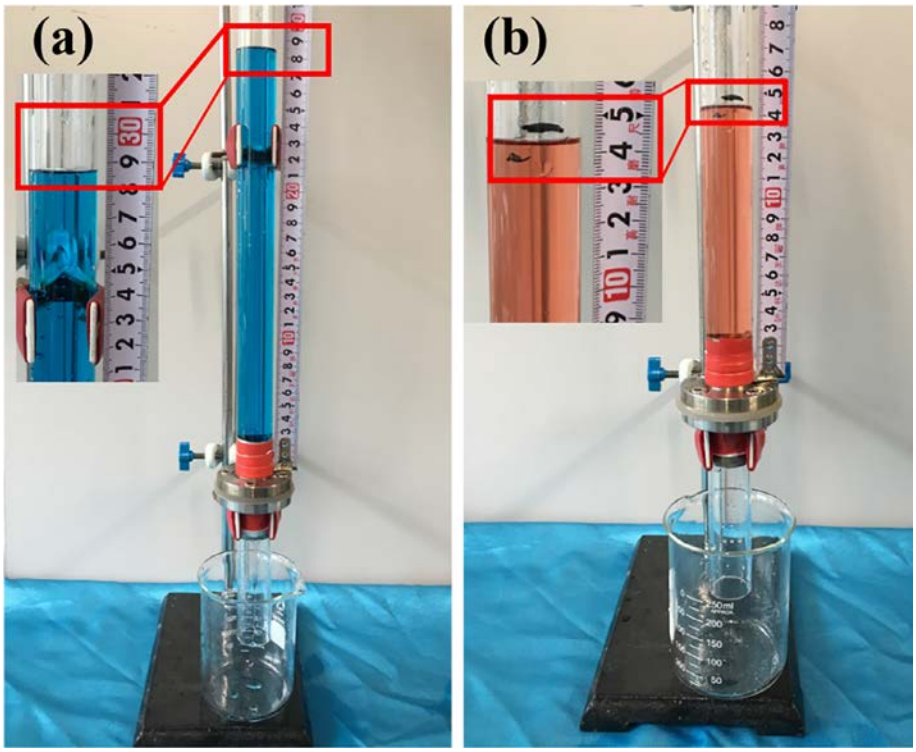

Fig. 1. The measurement of intrusion pressure of the SSM: (a) SSM@NWs-PFDS; (b) SSM@NWs.

and (2 0 0) crystal faces of the stainless steel, indicating that the original wire mesh is a high purity austenitic stainless steel [40]. Some new peaks are found on the basis of the austenite characteristic peaks after hydrothermal deposition and calcination (shown in black line of Fig. 5b). These new peaks are in agreement with the values of anatase TiO_2 [34]. Besides, the DXR Raman spectra (Fig. 5c) were further used to reveal the structure of nanowires. No significant absorption peaks were observed in spectrum of the pristine mesh and nanowires before annealing, demonstrating that TiO_2 nanowires treated under low temperature is an amorphous structure [41]. As for the nanowire structure after annealing, the typical absorption peaks at 144 cm^{-1}, 397 cm^{-1}, 521 cm^{-1} and 640 cm^{-1} corresponding to B_{1g}, Eg or Eg, B_{1g}, A_{1g} modes were assigned to anatase phase [42], indicating that the transformation from amorphous structure to anatase phase had been realized. XPS analysis was employed to explore surface composition, as shown in Fig. 5d. The original SSM was mainly composed of Fe, Cr, C, Si and O, meaning an alloy material. As for the surface of SSM@NWs, it was consist of Ti, O and C. Except for C, which affiliated to absorbed carbon specimen, the elements of Ti and O came from the TiO_2 nanowires structure. The high-resolution pattern of O 1 s was split into two peaks

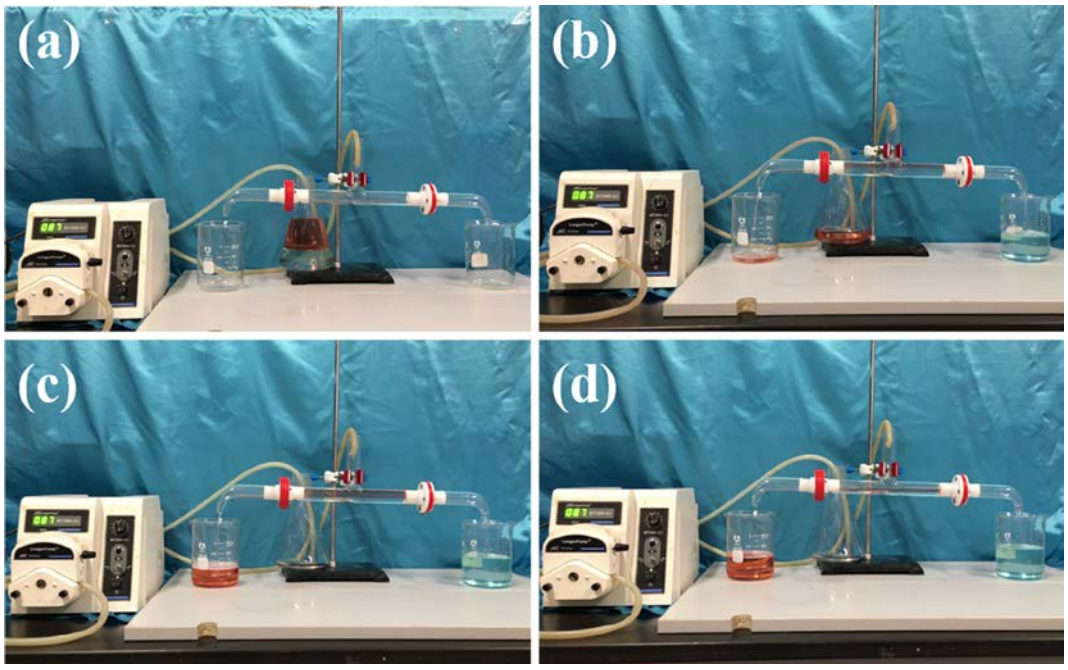

Fig. 2. The designed T-shaped bidirectional device integrated by two kinds of mesh with inverse wettability for continuous oil/water separation.

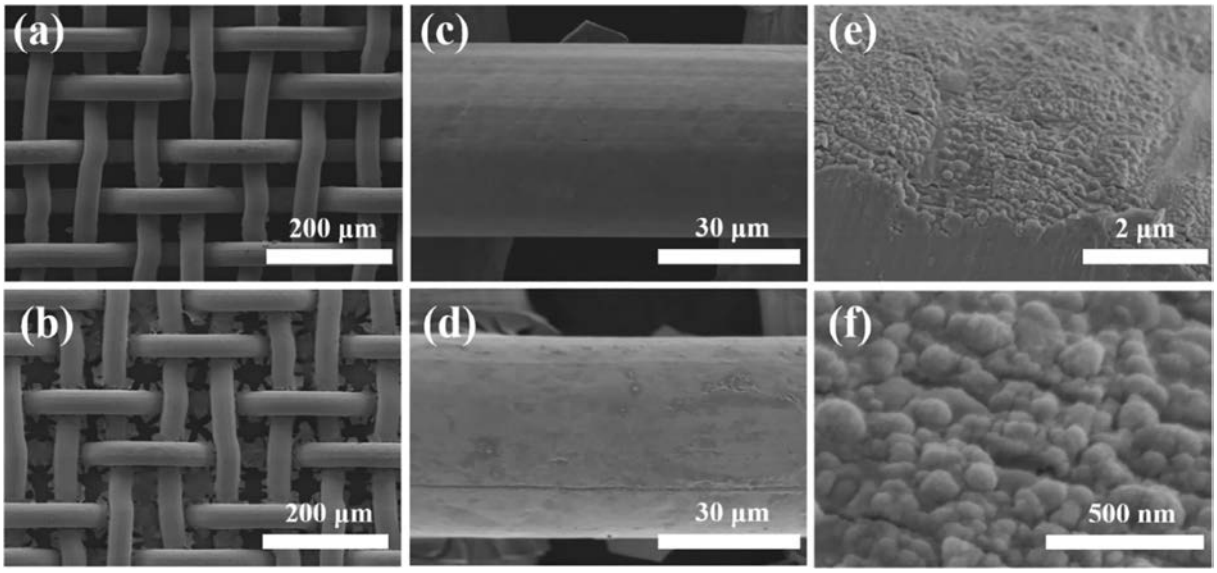

Fig. 3. SEM images of the pristine SSM (a), (c) and the SSM@SL (b), (d), (e), (f).

at 530.5 eV and 532 eV (Fig. 5e), which were in agreement with the binding energy of the lattice oxygen and the surface –OH groups, respectively [43]. The presence of hydroxyl groups on the surface is associated with oxygen vacancies or surface defect sites [44]. These sites may originate from the edge of the nanowires structure, dangling bonds and heat treatment process [45], which were capable of adsorbing hydroxyl groups dissociated by water molecules and thus enhanced the hydrophilicity of TiO_2. As depicted in Fig. 5f, the two peaks locating at 458.5 eV and 464.2 eV were related to the Ti $2p_{3/2}$ and Ti $2p_{1/2}$, respectively, which confirmed the existence of Ti^{4+} [46].

To test the wettability effect of superhydrophobic surface, a drop of water was dropped on the surface of the SSM@NWs-PFDS, as shown in Fig. 6a, it was clear that the water droplet exhibited a nearly ideal spherical shape. XPS characterization was also adopted to analyze the surface compositions by scanning binding energy of 0–1000 eV, and main elements of Ti, O, C, F and Si were included in SSM@NWs-PFDS (Fig. 6b). The EDS mapping results demonstrated that these elements were uniformly distributed on nanostructure surface of SSM@NWs-PFDS (Fig. S6). As shown in Fig. 6c, the high resolution signal of C 1s was split into three peaks at 294 eV, 291.5 eV and 285 eV corresponding to species of $–CF_3–$, $–CF_2–$ and C–C/C–H [47], respectively. The Si 2p file displaying the separated peaks at 102 eV and 103 eV (Fig. 6d) represents the bonds of Si–C and Si–O severally [48]. In addition, the surface structure was further explained by the O 1s profile, as shown in Fig. S7. These results imply that three-dimensional network structure was connected by Si-O-Si and the long-chain fluoroalkyl groups were successfully self-assembled on the TiO_2 surface, proving the significance of low surface energy modification to superhydrophobic formation.

3.3. Wettability of the meshes

The surface of the original mesh is silvery white, as shown in Fig. 7a. The water contact angle (WCA) in air is 119°, which far reaches the superhydrophobic standard. However, the oil contact angles (OCA) in air and underwater are 32° and 126°, respectively, demonstrating that the original mesh has the properties of oleophilicity in air and oleophobicity underwater. For SSM@NWs, the coating could result in amphipathicity in air owing to the connatural hydrophilic property of TiO_2

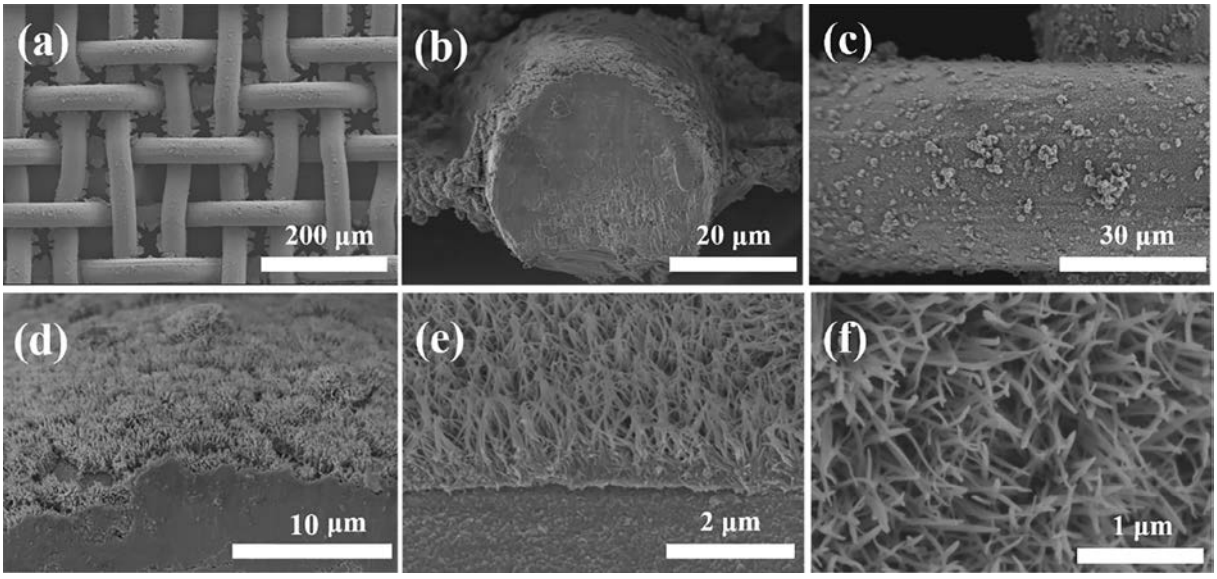

Fig. 4. SEM images of the surface morphology of the SSM@NWs.

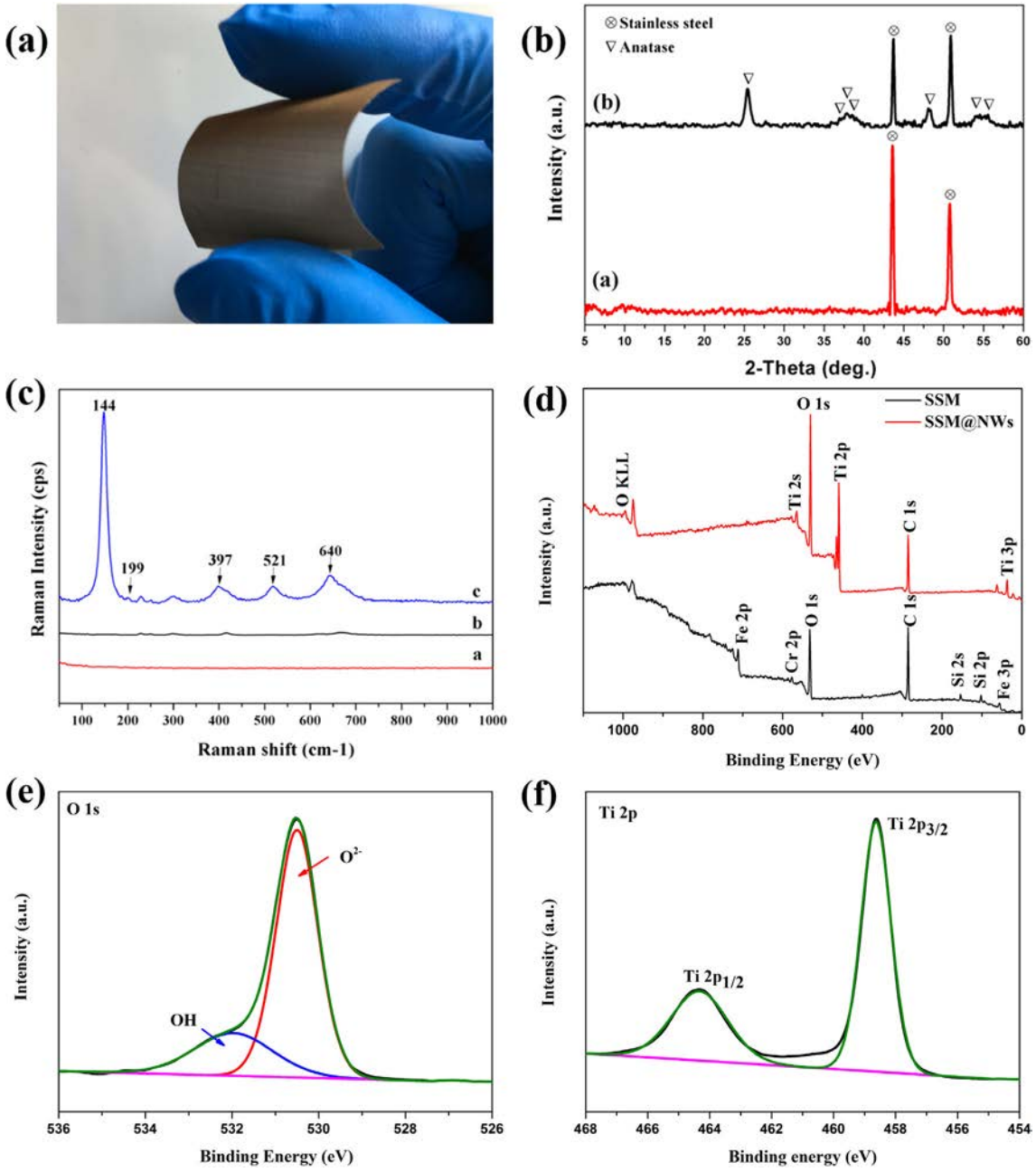

Fig. 5. (a) A photo of the as-prepared SSM@NWs; (b) XRD patterns: a. pristine SSM, b. the as-prepared SSM@NWs; (c) Raman spectrum: a. pristine SSM, b. nanowire structures before annealing, c. nanowire structures after annealing; (d) The full spectrum of original SSM and SSM@NWs; High-resolution XPS analysis: (e) O 1s and (f) Ti 2p of the SSM@NWs.

and increased hierarchical roughness. When the superhydrophilic mesh was wetted by water, a thin water-solid interface formed on nanowires structure, which served as the protective layer to avoid a large area contact between the oil and the SSM@NWs [31]. As a consequence, the SSM@NWs demonstrated a high OCA underwater of 156° (Fig. 7b). By changing the surface composition, the WCA of SSM@NWs-PFDS were measured to be 158° in air and 155° under oil, showing the excellent superhydrophobic performance (shown in Fig. 7c). The high WCA on SSM@NWs-PFDS was indicators of the Cassie-Baxter models, which could be accounted for the hierarchical structure [49]. Meanwhile, the oil droplets wetted and penetrated the mesh channels upon being injected to the surface, suggesting high affinity of the modified mesh to the oil phase.

To study the dynamic wettability between the superwetting surface and the droplets, a high-speed camera was employed to observe the changes in state of 5 μL droplet at different time. The pristine surface possessed a greater adhesion to water and water droplet was adhered to the vertical position (Fig. 8a). By contrast, the dripping water droplet bounced off and rolled down the superhydrophobic surface within 32 ms (Fig. 8b). Significantly, the low adhesion between the water and SSM@NWs-PFDS could result in the “lotus leaf phenomenon”, thus demonstrating its self-cleaning effect [38]. Moreover, the oil droplet was also performed on the tilted surface of pristine mesh (Fig. 8c) and superhydrophilic mesh (Fig. 8d) under water. It could be noticed that the oil droplet was anchored on the middle position of the original mesh after scrolling a certain distance, implying a relatively large adhesion to oil. However, for TiO_2 nanowires coated mesh, it showed a splendid underwater superoleophobicity with a complete spherical oil drop remaining on surface. This characterization resembling the fish scale, which can protect the as-prepared superhydrophilic surface from the

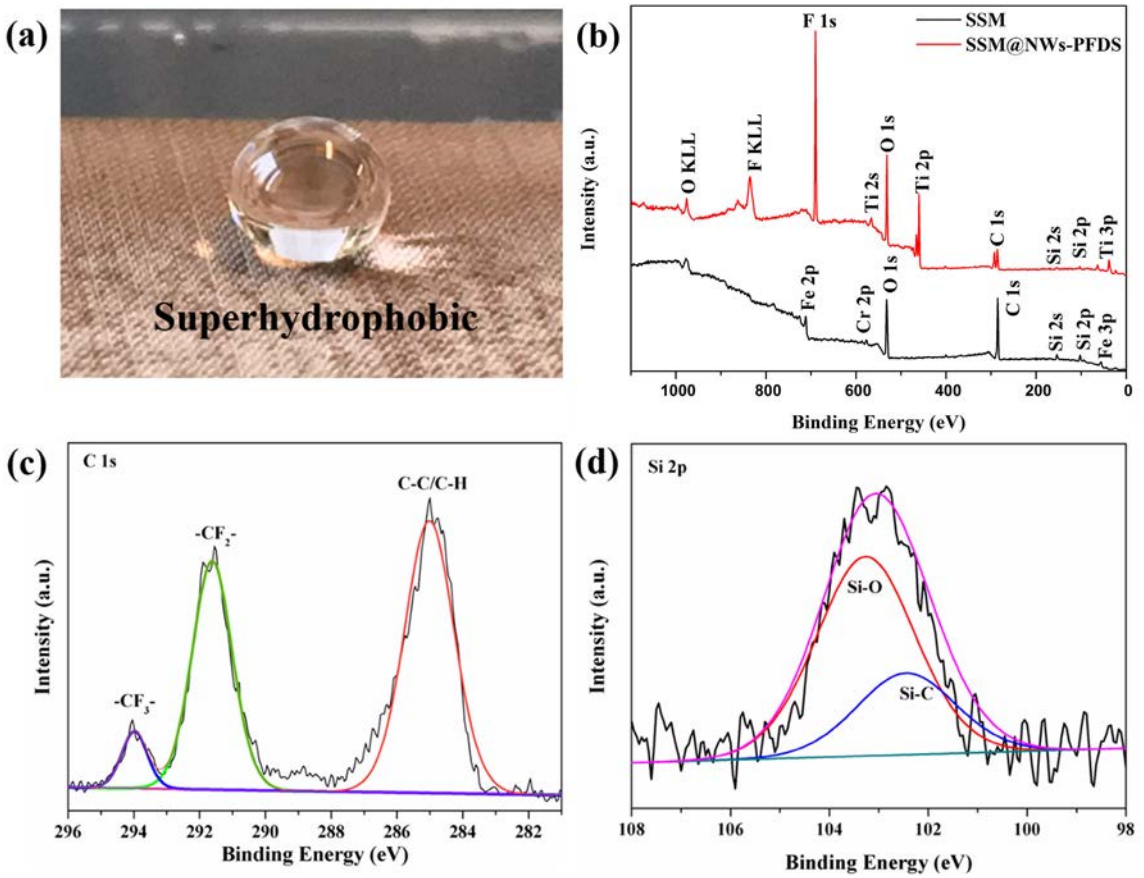

Fig. 6. (a) A photo of the SSM@NWs-PFDS; XPS spectra: (b) the survey of original SSM and SSM@NWs-PFDS, the peak fitting of (c) C 1s and (d) Si 2p of SSM@NWs-PFDS.

contamination of oil [31].

A series of experiments were carried out to verify the special wetting behavior. As shown in Fig. 9a, various types of droplets were settled on the surface of the SSM@NWs-PFDS and exhibited non-wetting state with a nearly spherical shape, endowing the superhydrophobic surface with the anti-corrosion property due to the existence of air cushion captured in the hierarchical structure. Using the water column to flush the surface of SSM@NWs-PFDS, it would bounce off quickly without leaving any trace (Fig. 9b), confirming the low adhesion feature of surface again. Furthermore, the Cassie-Baxter non-wetting status was shown by the transparent "mirror" phenomenon observed beneath the water when the original mesh and SSM@NWs-PFDS were attached on

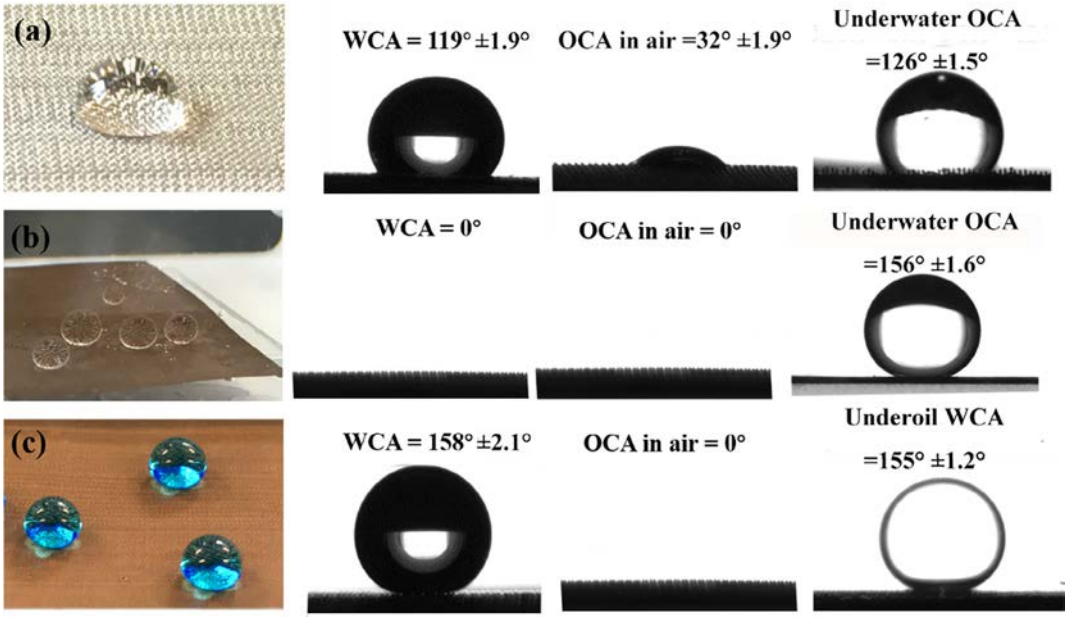

Fig. 7. Contact angles measurement: (a) pristine SSM, (b) SSM@NWs, (c) SSM@NWs-PFDS.

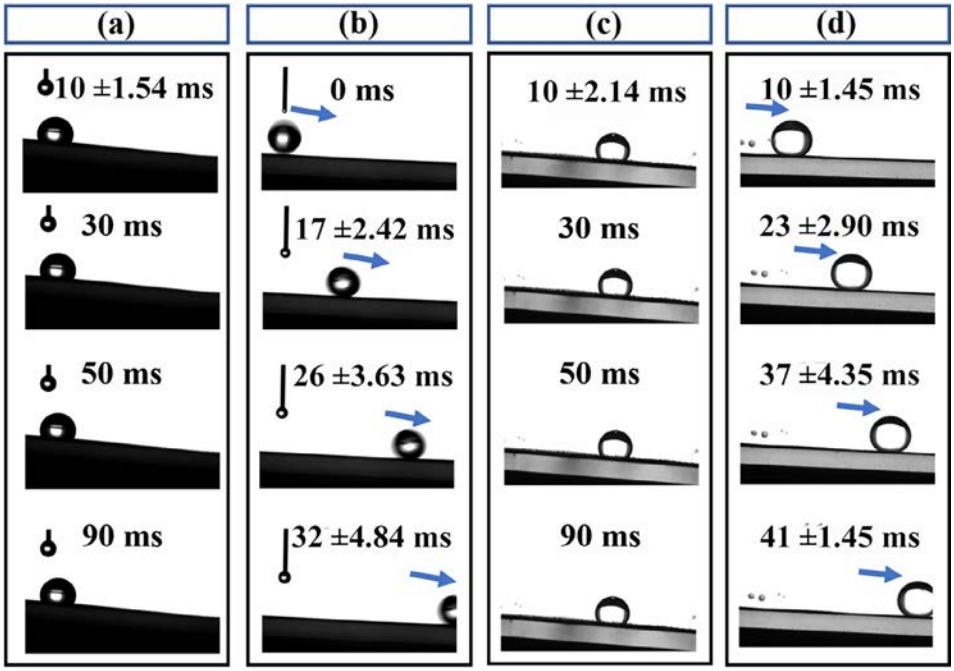

Fig. 8. Adhesion test: (a) a drop of water dropped onto the pristine SSM and (b) the SSM@NWs-PFDS; (c) A drop of oil underwater dropped onto the pristine SSM and (d) the SSM@NWs.

the glass sheet and immersed in water (Fig. 9c–d). The superhydrophobicity and the presence of air bubbles at the interface allowed the SSM@NWs-PFDS to float on the surface while the original one sank into the water (Fig. 9e). It is obvious that SSM@NWs-PFDS would suspend at the oil/water interface when adding oil to the beaker continually (Fig. 9f). All above results implied the ultralow adhesion of water to the superhydrophobic surface.

3.4. Oil/water separation ability

A variety of oil/water mixtures, including n-hexane/water, diesel/water, petroleum ether/water, kerosene/water and dichloromethane/water, were separated in sequence by detailed separation device (Fig. 2). The results demonstrated that a pair of as-prepared meshes showed high separation efficiencies ranging from 99% to 99.5% for a series of oil/water mixtures (Fig. 10a–b), indicating an excellent separation performance. Due to the similar viscosity and density between

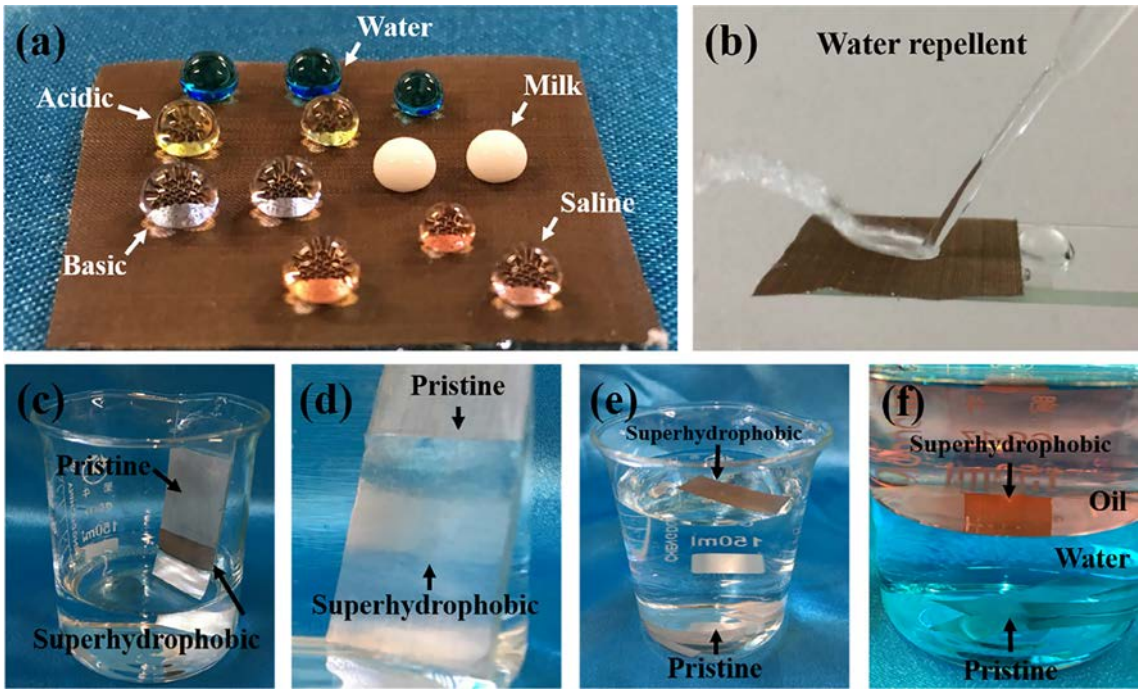

Fig. 9. (a) Different kinds of droplets on the surface of the SSM@NWs-PFDS; (b) A jet of water was bounced off by the surface of the SSM@NWs-PFDS; (c) (d) The pristine SSM and SSM@NWs-PFDS were immersed into the water; (e) The SSM@NWs-PFDS floated on the surface of water while the pristine SSM sank to bottom; (f) The as-prepared SSM@NWs-PFDS suspended at the interface of oil and water while the pristine SSM sank to bottom.

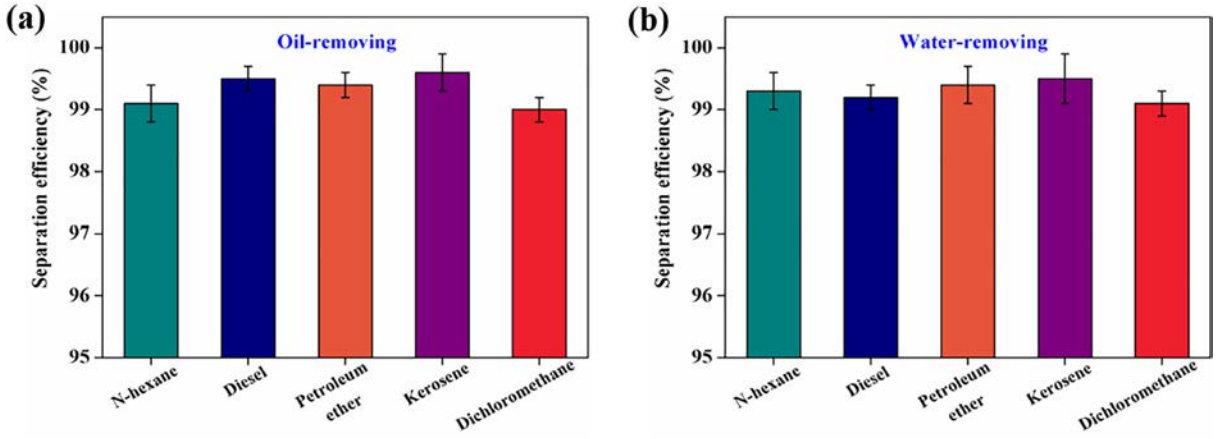

Fig. 10. The oil/water separation efficiency: (a) SSM@NWs-PFDS; (b) SSM@NWs.

the sample oils [31], there is a negligible difference with separation efficiency. For practical application, the desired separation selectivity is beneficial from the high separation efficiency [4].

Besides, the permeation flux is also a crucial parameter to evaluate the realistic separation effect. We calculated the permeation flux by measuring the volume of collected water or oil over a period of time with a formula.

$$Flux = V/(S \times t) \quad (5)$$

where V is the volume of water or oil that passed through the mesh, S represents the effective contact area (3.1 cm^2) and t is separation time. Here, the water flux was measured to be 4.5 $L\,m^{-2}\,s^{-1}$, and other oil fluxes were shown in Fig. S4. It can be observed that the flux for petroleum ether was up to 7 $L\,m^{-2}\,s^{-1}$ and other oils were measured to be higher than 4 $L\ m^{-2}\ s^{-1}$. According to the reported viscosity relationship between the oils and water [31], it is speculated that the continuous phase penetrating the meshed with relatively high viscosity has a large flow resistance and low permeation flux, which is consistent with our experimental results. The fluid flux could remain high under the condition of low viscosity, which provided the instructive significance for liquid manipulation.

On account of the above discussed results, the remarkable separation efficiency and flux were obtained for various oils, which is vital for achieving the large-scale oil/water separation.

3.5. The durability of the meshes

The durability for repeated use was briefly assessed by observing the surface morphology of SSM@NWs with different cycles. After each separation operation (kerosene/water, 1 L, 1:1 of volume ratio), the used meshes were cleaned with ethanol and then dried at ambient environment, followed by another reuse. With the increase of use cycles, the spherical particles on surface were gradually reduced to a certain amount (Fig. 11a–c). It is obvious that when the repeated cycles reached to 50, only a small amount of rough particles could be seen (Fig. 11c). These particles were result of secondary growth of the crystal on the surface of the nanowires, which fell off after repeated washing and scouring procedure. Moreover, the reused mesh with 50 cycles still maintained the super wettability with WCA of 151° for SSM@NWs-PFDS and underwater OCA of 152° for SSM@NWs (Fig. 11d), meaning that the formed TiO_2 nanowires did not change significantly (insert in Fig. 11c).

3.6. Industrial implications of the developed materials

In a realistic separation process, the admirable anti-corrosion property is an important factor to achieve continuous oil/water separation. The chemical stability of the as-prepared mesh in extreme conditions was tested and then measured by contact angle and separation efficiency. The concrete corrosive solution was set as follows: acidic and alkaline solution with a wide pH range of 1–14 and saline NaCl solution with a mass concentration of 0–10%. Afterwards, the SSM@NWs and SSM@NWs-PFDS were immersed in corrosive solution for 24 h, and then the wettability performance and capability of oil/water separation were measured. As illustrated as Fig. 12a, the contact angles for both kinds of meshes were all above 150° and separation efficiencies were more than 98.5%. Furthermore, after treated in saline solution, the contact angle exceeded 150° and the separation efficiencies remained higher than 99% (Fig. 12b). It indicated that the nanowire structure of the mesh prepared in our work has particular corrosion resistance in harsh conditions set by the experiment.

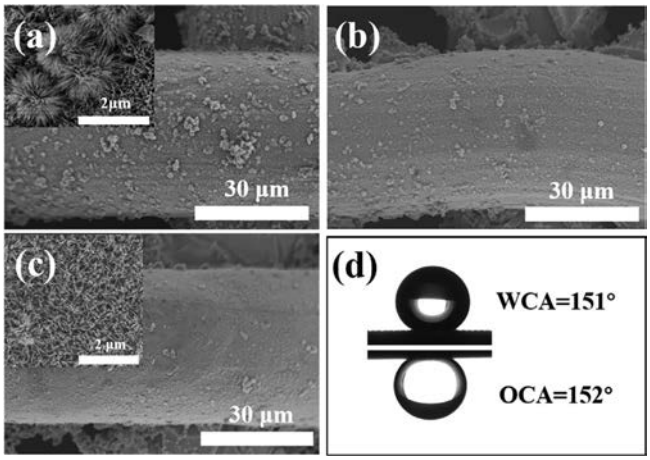

Fig. 11. SEM images of SSM@NWs for repeated use: (a) 0 cycle; (b) 25 cycles; (c) 50 cycles. (d) The WCA of SSM@NWs-PFDS and the underwater OCA of SSM@NWs after 50 reuse cycles.

In consideration of the complexity of industrial oily wastewater, the surface morphologies of SSM@NWs immersed in corrosive solution, including 0.1 M and 1 M HCl, 0.1 M and 1 M NaOH as well as 10% NaCl for 24 h were studied (detail in Fig. S5). Especially, the acanthosphere-like structure could be seen after etching in 1 M NaOH solution, which may lies in that TiO_2 was dissolved and recrystallized in solution, further producing these novel structure on surface. Finally, we can conclude that the nanowire structure fabricated in our work has good corrosion resistance to the lower concentration of chemical solution, while the highly acidic or alkaline environment will damage the microstructure of the superhydrophilic surface.

Generally speaking, the industrial environment tends to be rigorous.

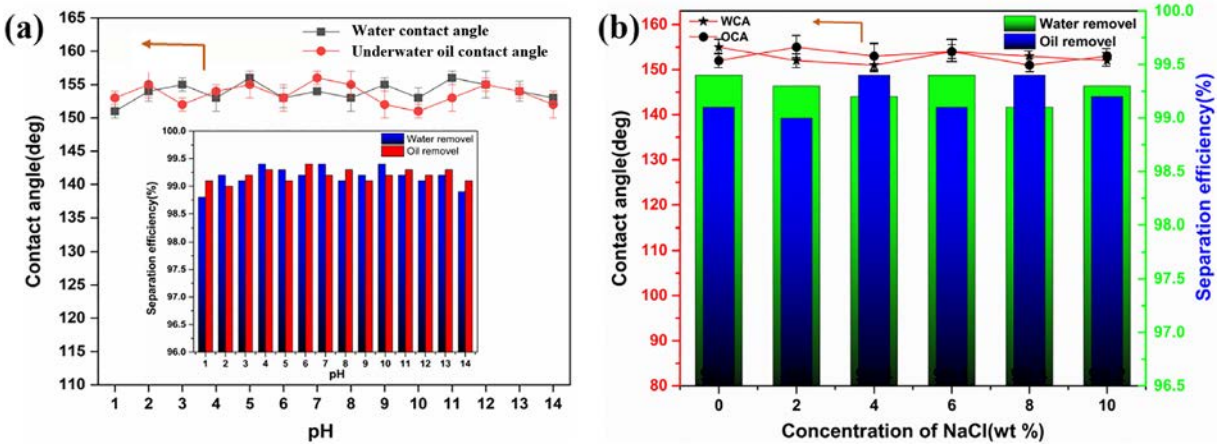

Fig. 12. Influence of solution with (a) different pH and (b) saline environment on the wettability and separation efficiency of SSM@NWs and SSM@NWs-PFDS.

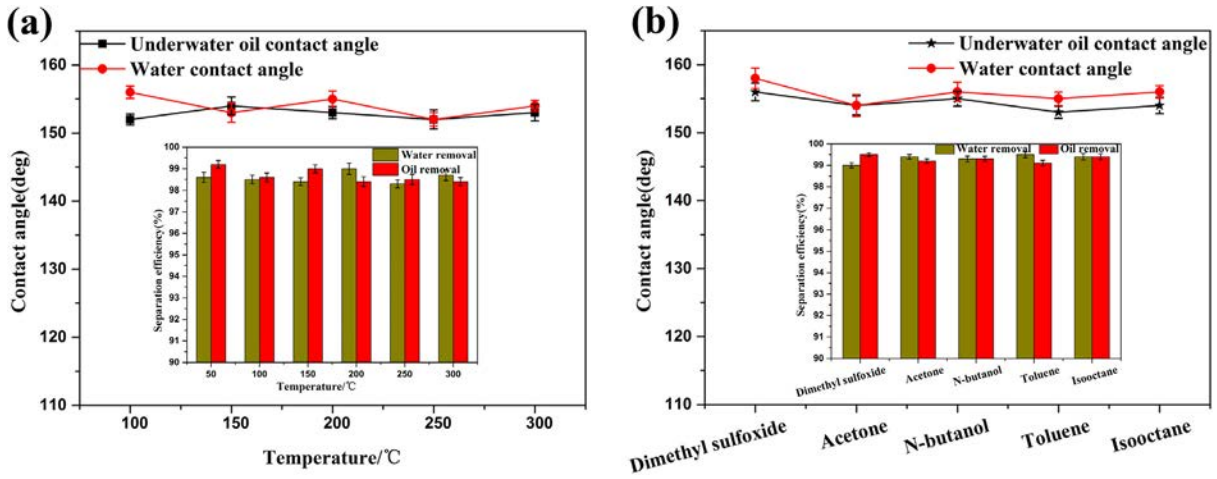

Fig. 13. Effect of (a) temperatures and (b) organic solvents on the contact angles and separation efficiency of the as-prepared mesh.

The influence of high temperature conditions and corrosive organic solvents on the performance of the as-prepared meshes will determine their using life, which directly impacts the economic cost of the application. The contact angle and petroleum ether/water separation efficiency of the meshes after treatment under different temperature conditions for 6 h were measured, and the results are demonstrated in Fig. 13a. It is clear that there is no obvious fluctuation in terms of the contact angles and separation efficiency, signifying that the as-prepared meshes have the excellent thermal stability. Various organic solvent, including dimethyl sulfoxide (DMSO), acetone, n-butanol, toluene and isooctane, were employed as the organic environment. Then, the as-prepared meshes were immersed in different solvents for 48 h. The results (Fig. 13b) suggested that superhydrophilic and superhydrophobic meshes maintained high values for surface wettability performance and separation efficiency after the immersion treatment. Owing to the intrinsic stability of TiO_2 and covalent bonds between PFDS molecules and TiO_2 surface, it can be concluded that the excellent properties were ascribed to the strong interaction among multilayers. The remarkable durability, as well as excellent stability in various condition could guarantee the long-term use, which is favorable to minimize the replacement cost of the material. Besides, the energy consumption was reduced in some degree when adopting the low temperature hydrothermal method. More importantly, the raw materials with low price synthesized for separation filters are of great significance in practical application. However, the large-scale production requirement for separation filters with hydrothermal approach still suffer the severe challenge. In summary, our work provide a brand new method for fabricating the meshes with inverse wettability, which paves the way for manufacture of highly waterproof materials, as well as the application in anti-corrosion and self-cleaning surface.

4. Conclusion

In summary, our work is based on the structure-induced superhydrophilic mechanism. The growth of TiO_2 nanowire structure on the surface of mesh was realized by seed layer deposition and hydrothermal method. The superhydrophilic mesh was then converted into the superhydrophobic one via a facile modification to lower the surface energy. Importantly, the as-designed continuous oil/water separation device integrated the two meshes consisting of the inverse wettability, and the separation efficiencies of various oil/water mixtures were all above 99%, showing a high separation flux simultaneously. Furthermore, the device can avoid the limitation of density relationship and overplus of repulsive phase accumulated in oil/water separation process. Even treated in harsh condition, such as acidic and alkaline aqueous solution, salty solution, high temperature and organic solvents, the as-obtained meshes could maintain high separation efficiency greater than 98%. After repeated use for 50 cycles, no obvious variations of microscopic morphology were observed on surface of SSM@NWs. As a result, it is believed that the ideal stability could expand its application in self-cleaning surface, synthesis of drag reducing material, fluidic equipment and oil/water separation etc.

Acknowledgment

We are grateful for the financial support from National Key R&D Program of China (No. 2016YFC0400406).

Appendix A. Supplementary data

Supplementary data to this article can be found online at https://doi.org/10.1016/j.cej.2019.122524.

References

[1] J. He, B. Li, H. Wu, K. Kulasinski, M. Mao, W. Jiang, J. Niu, Interaction of miscible solutions and superhydrophobic surfaces, Surf. Eng. 35 (2018) 387–393.
[2] R.A. Kerr, A lot of oil on the loose, Not so much to be found, Science 329 (2010) 734–735.
[3] H. Wang, J. Yang, X. Liu, Z. Tao, Z. Wang, R. Yue, A robust 3D superhydrophobic sponge for in situ continuous oil removing, J. Mater. Sci. 54 (2018) 1255–1266.
[4] B. Jiang, H. Zhang, Y. Sun, L. Zhang, L. Xu, L. Hao, H. Yang, Covalent layer-by-layer grafting (LBLG) functionalized superhydrophobic stainless steel mesh for oil/water separation, Appl. Surf. Sci. 406 (2017) 150–160.
[5] Lei Zhai, Michael C. Berg, F.Ç. Cebeci, Yushan Kim, John M. Milwid, Michael F. Rubner, Robert E. Cohen, Patterned superhydrophobic surfaces: toward a synthetic mimic of the Namib Desert Beetle, Nano Lett. 6 (2015) 1213–1217.
[6] L. Feng, Z. Zhang, Z. Mai, Y. Ma, B. Liu, L. Jiang, D. Zhu, A super-hydrophobic and super-oleophilic coating mesh film for the separation of oil and water, Angew. Chem.-Int. Edit. 43 (2004) 2012–2014.
[7] L. Zhang, L. Xu, Y. Sun, N. Yang, Robust and durable superhydrophobic polyurethane sponge for oil/water separation, Ind. Eng. Chem. Res. 55 (2016) 11260–11268.
[8] E.-C. Cho, C.-W. Chang-Jian, H.-C. Chen, K.-S. Chuang, J.-H. Zheng, Y.-S. Hsiao, K.-C. Lee, J.-H. Huang, Robust multifunctional superhydrophobic coatings with enhanced water/oil separation, self-cleaning, anti-corrosion, and anti-biological adhesion, Chem. Eng. J. 314 (2017) 347–357.
[9] Z. Zhang, B. Ge, X. Men, Y. Li, Mechanically durable, superhydrophobic coatings prepared by dual-layer method for anti-corrosion and self-cleaning, Colloid Surf. A-Physicochem. Eng. Asp. 490 (2016) 182–188.
[10] X. Liu, L. Ge, W. Li, X. Wang, F. Li, Layered double hydroxide functionalized textile for effective oil/water separation and selective oil adsorption, ACS Appl. Mater. Interfaces 7 (2015) 791–800.
[11] L. Zhou, P. Yu, Y. He, H. Xia, X. Guo, Y. Luo, A facile dip-coating approach to stable superhydrophobic SiO2/epoxy resin membrane preparation for micro-water separation in transformer oil liquids, RSC Adv. 5 (2015) 92947–92953.
[12] C. Zhang, Y. Li, N. Bai, C. Tan, P. Cai, Q. Li, Fabrication of robust 3D superhydrophobic material by a simple and low-cost method for oil-water separation and oil absorption, Mater. Sci. Eng. B-Adv. Funct. Solid-State Mater. 224 (2017) 117–124.
[13] E. Wang, H. Wang, Z. Liu, R. Yuan, Y. Zhu, One-step fabrication of a nickel foam-based superhydrophobic and superoleophilic box for continuous oil–water separation, J. Mater. Sci. 50 (2015) 4707–4716.
[14] X. Chen, Y. He, Y. Fan, Q. Yang, G. Zeng, H. Shi, Facile fabrication of a robust superwetting three-dimensional (3D) nickel foam for oil/water separation, J. Mater. Sci. 52 (2016) 2169–2179.
[15] Z. Wang, S. Ji, F. He, M. Cao, S. Peng, Y. Li, One-step transformation of highly hydrophobic membranes into superhydrophilic and underwater superoleophobic ones for high-efficiency separation of oil-in-water emulsions, J. Mater. Chem. A 6 (2018) 3391–3396.
[16] S.K. Hong, S. Bae, H. Jeon, M. Kim, S.J. Cho, G. Lim, An underwater superoleophobic nanofibrous cellulosic membrane for oil/water separation with high separation flux and high chemical stability, Nanoscale 10 (2018) 3037–3045.
[17] F. Lu, Y. Chen, N. Liu, Y. Cao, L. Xu, Y. Wei, L. Feng, A fast and convenient cellulose hydrogel-coated colander for high-efficiency oil–water separation, RSC Adv. 4 (2014) 32544–32548.
[18] C. Ao, R. Hu, J. Zhao, X. Zhang, Q. Li, T. Xia, W. Zhang, C. Lu, Reusable, salt-tolerant and superhydrophilic cellulose hydrogel-coated mesh for efficient gravity-driven oil/water separation, Chem. Eng. J. 338 (2018) 271–277.
[19] Y. Gu, J. Yang, S. Zhou, A facile immersion-curing approach to surface-tailored poly (vinyl alcohol)/silica underwater superoleophobic coatings with improved transparency and robustness, J. Mater. Chem. A 5 (2017) 10866–10875.
[20] M. Zeng, B. Peng, C. Ybanez, N.W. Tan, E.A. Deeb, E. Bordovsky, C.-H. Choi, I. Echols, A. Nguyen, A. Ye, N. Dendumrongsup, L. Zhang, D. Huang, P. Wang, J. Luo, Y. Situ, Z. Cheng, High-flux underwater superoleophobic hybrid membranes for effective oil–water separation from oil-contaminated water, RSC Adv. 7 (2017) 9051–9056.
[21] J. Ge, J. Zhang, F. Wang, Z. Li, J. Yu, B. Ding, Superhydrophilic and underwater superoleophobic nanofibrous membrane with hierarchical structured skin for effective oil-in-water emulsion separation, J. Mater. Chem. A 5 (2017) 497–502.
[22] M. Liu, S. Wang, Z. Wei, Y. Song, L. Jiang, Bioinspired design of a superoleophobic and low adhesive water/solid interface, Adv. Mater. 21 (2009) 665–669.
[23] J. Liu, L. Wang, N. Wang, F. Guo, L. Hou, Y. Chen, J. Liu, Y. Zhao, L. Jiang, A robust Cu(OH)2 nanoneedles mesh with tunable wettability for nonaqueous multiphase liquid separation, Small 13 (2017).
[24] L. Yan, J. Li, W. Li, F. Zha, H. Feng, D. Hu, A photo-induced ZnO coated mesh for on-demand oil/water separation based on switchable wettability, Mater. Lett. 163 (2016) 247–249.
[25] J. Li, L. Yan, W. Li, J. Li, F. Zha, Z. Lei, Superhydrophilic–underwater superoleophobic ZnO-based coated mesh for highly efficient oil and water separation, Mater. Lett. 153 (2015) 62–65.
[26] X. Lin, F. Lu, Y. Chen, N. Liu, Y. Cao, L. Xu, Y. Wei, L. Feng, One-step breaking and separating emulsion by tungsten oxide coated mesh, ACS Appl. Mater. Interfaces 7 (2015) 8108–8113.
[27] M.A. Gondal, M.S. Sadullah, M.A. Dastageer, G.H. Mckinley, D. Panchanathan, K.K. Varanasi, Study of factors governing oil-water separation process using TiO_2 films prepared by spray deposition of nanoparticle dispersions, ACS Appl. Mater. Interfaces 6 (2014) 13422–13429.
[28] M. Yang, W. Liu, C. Jiang, C. Liu, S. He, Y. Xie, Z. Wang, Facile preparation of robust superhydrophobic cotton textile for self-cleaning and oil-water separation, Ind. Eng. Chem. Res. 58 (2018) 187–194.
[29] A. Fujishima, X. Zhang, D. Tryk, TiO2 photocatalysis and related surface phenomena, Surf. Sci. Rep. 63 (2008) 515–582.
[30] N. Sakai, A. Fujishima, T. Watanabe, K. Hashimoto, Quantitative evaluation of the photoinduced hydrophilic conversion properties of TiO2 thin film surfaces by the reciprocal of contact angle, J. Phys. Chem. B 107 (2003) 1028–1035.
[31] B. Jiang, Z. Chen, H. Dou, Y. Sun, H. Zhang, Z.Q. Gong, L. Zhang, Superhydrophilic and underwater superoleophobic Ti foam with fluorinated hierarchical flower-like TiO 2 nanostructures for effective oil-in-water emulsion separation, Appl. Surf. Sci. 456 (2018) 114–123.
[32] A. Galan-Gonzalez, A. Gallant, D.A. Zeze, D. Atkinson, Controlling the growth of single crystal ZnO nanowires by tuning the atomic layer deposition parameters of the ZnO seed layer, Nanotechnology 30 (2019) 305602.
[33] J.-M. Wu, H.-X. Xue, Photocatalytic active titania nanowire arrays on Ti substrates, J. Am. Ceram. Soc. 92 (2009) 2139–2143.
[34] Y. Xiong, M. Lai, J. Li, H. Yong, H. Qian, C. Xu, K. Zhong, S. Xiao, Facile synthesis of ultra-smooth and transparent TiO2 thin films with superhydrophilicity, Surf. Coat. Technol. 265 (2015) 78–82.
[35] C. Chen, B. Wang, H. Liu, T. Chen, H. Zhang, J. Qiao, Synthesis of 3D dahlia-like Co3O4 and its application in superhydrophobic and oil-water separation, Appl. Surf. Sci. 471 (2019) 289–299.
[36] J.b. Zhong, J.z. Li, F.m. Feng, S.t. Huang, J. Zeng, CTAB-assisted fabrication of TiO2 with improved photocatalytic performance, Mater. Lett. 100 (2013) 195–197.
[37] B. Liu, J.E. Boercker, E.S. Aydil, Oriented single crystalline titanium dioxide nanowires, Nanotechnology 19 (2008) 505604.
[38] J. Rong, T. Zhang, F. Qiu, J. Xu, Y. Zhu, D. Yang, Y. Dai, Design and preparation of efficient, stable and superhydrophobic copper foam membrane for selective oil absorption and consecutive oil–water separation, Mater. Des. 142 (2018) 83–92.
[39] X. Liu, Z. Jin, S. Bu, J. Zhao, Z. Liu, Effect of buffer layer on solution deposited ZnO films, Mater. Lett. 59 (2005) 3994–3999.
[40] Y. Chen, D.D. Dionysiou, TiO2 photocatalytic films on stainless steel: The role of Degussa P-25 in modified sol–gel methods, Appl. Catal. B-Environ. 62 (2006) 255–264.
[41] Y.H. Zhang, C.K. Chan, J.F. Porter, G. Wei, Micro-Raman spectroscopic characterization of nanosized TiO2 powders prepared by vapor hydrolysis, J. Mater. Res. 13 (1998) 8.
[42] W.F. Zhang, Y.L. He, M.S. Zhang, Z. Yin, Q. Chen, Raman scattering study on anatase TiO2 nanocrystals, J. Phys. D-Appl. Phys. 33 (2000) 912.
[43] Y. Li, T. Sasaki, Y. Shimizu, N. Koshizaki, A hierarchically ordered TiO2 hemispherical particle array with hexagonal-non-close-packed tops: synthesis and stable superhydrophilicity without UV irradiation, Small 4 (2008) 2286–2291.
[44] R. Wang, K. Hashimoto, A. Fujishima, M. Chikuni, E. Kojima, A. Kitamura, M. Shimohigoshi, T. Watanabe, Light-induced amphiphilic surfaces, Nature 388 (1997) 431–432.
[45] L.U. Gq, A. Linsebigler, J.T. Yates, Ti3+ defect sites on TiO2(110): production and chemical detection of active sites, J. Phys. Chem. 98 (1947) 155–157.
[46] X. Lu, G. Wang, T. Zhai, M. Yu, J. Gan, Y. Tong, Y. Li, Hydrogenated TiO2 nanotube arrays for supercapacitors, Nano Lett. 12 (2012) 1690–1696.
[47] Z. Duan, Z. Zhao, D. Luo, M. Zhao, G. Zhao, A facial approach combining photosensitive solgel with self-assembly method to fabricate superhydrophobic TiO2 films with patterned surface structure, Appl. Surf. Sci. 360 (2016) 1030–1035.
[48] M. Qu, X. Ma, J. He, J. Feng, S. Liu, Y. Yao, L. Hou, X. Liu, Facile selective and diverse fabrication of superhydrophobic, superoleophobic-superhydrophilic and superamphiphobic materials from kaolin, ACS Appl. Mater. Interfaces 9 (2017) 1011–1020.
[49] E. Bormashenko, Progress in understanding wetting transitions on rough surfaces, Adv. Colloid Interface Sci. 222 (2015) 92–103.